Journal for ImmunoTherapy of Cancer

BRD4 inhibition impairs DNA mismatch repair, induces mismatch repair mutation signatures and creates therapeutic vulnerability to immune checkpoint blockade in MMR-proficient tumors

Yu Fu,[1,2] Bin Yang,[1,2] Yaoyuan Cui,[1,2] Xingyuan Hu,[1,2] Xi Li,[1,2] Funian Lu,[1,2] Tianyu Qin,[1,2] Li Zhang,[1,2] Zhe Hu ,[1,2] Ensong Guo,[1,2] Junpeng Fan,[1,2] Rourou Xiao,[3] Wenting Li,[1,2,4] Xu Qin,[2,5] Dianxing Hu,[1,2] Wenju Peng,[1,2] Jingbo Liu,[1,2] Beibei Wang,[1,2] Gordon B Mills,[6] Gang Chen,[1,2] Chaoyang Sun [1,2]

To cite: Fu Y, Yang B, Cui Y, *et al*. BRD4 inhibition impairs DNA mismatch repair, induces mismatch repair mutation signatures and creates therapeutic vulnerability to immune checkpoint blockade in MMR-proficient tumors. *Journal for ImmunoTherapy of Cancer* 2023;**11**:e006070. doi:10.1136/jitc-2022-006070

► Additional supplemental material is published online only. To view, please visit the journal online (http://dx.doi.org/10.1136/jitc-2022-006070).

Accepted 20 March 2023

For numbered affiliations see end of article.

Correspondence to
Professor Chaoyang Sun; suncydoctor@gmail.com

ABSTRACT

Background Mismatch repair deficiency (dMMR) is a well-recognized biomarker for response to immune checkpoint blockade (ICB). Strategies to convert MMR-proficient (pMMR) to dMMR phenotype with the goal of sensitizing tumors to ICB are highly sought. The combination of bromodomain containing 4 (BRD4) inhibition and ICB provides a promising antitumor effect. However, the mechanisms underlying remain unknown. Here, we identify that BRD4 inhibition induces a persistent dMMR phenotype in cancers.

Methods We confirmed the correlation between BRD4 and mismatch repair (MMR) by the bioinformatic analysis on The Cancer Genome Atlas and Clinical Proteomic Tumor Analysis Consortium data, and the statistical analysis on immunohistochemistry (IHC) scores of ovarian cancer specimens. The MMR genes (MLH1,MSH2,MSH6,PMS2) were measured by quantitative reverse transcription PCR, western blot, and IHC. The MMR status was confirmed by whole exome sequencing, RNA sequencing, MMR assay and hypoxanthine-guanine phosphoribosyl transferase gene mutation assay. The BRD4i AZD5153 resistant models were induced both in vitro and in vivo. The transcriptional effects of BRD4 on MMR genes were investigated by chromatin immunoprecipitation among cell lines and data from the Cistrome Data Browser. The therapeutic response to ICB was testified in vivo. The tumor immune microenvironment markers, such as CD4, CD8, TIM-3, FOXP3, were measured by flow cytometry.

Results We identified the positive correlation between *BRD4* and MMR genes in transcriptional and translational aspects. Also, the inhibition of BRD4 transcriptionally reduced MMR genes expression, resulting in dMMR status and elevated mutation loads. Furthermore, prolonged exposure to AZD5153 promoted a persistent dMMR signature both in vitro and in vivo, enhancing tumor immunogenicity, and increased sensitivity to α-programmed death ligand-1 therapy despite the acquired drug resistance.

Conclusions We demonstrated that BRD4 inhibition suppressed expression of genes critical to MMR, dampened MMR, and increased dMMR mutation signatures both in vitro and in vivo, sensitizing pMMR tumors to ICB. Importantly, even in BRD4 inhibitors (BRD4i)-resistant tumor models, the effects of BRD4i on MMR function were maintained rendering tumors sensitive to ICB. Together, these data identified a strategy to induce dMMR in pMMR tumors and further, indicated that BRD4i sensitive and resistant tumors could benefit from immunotherapy.

WHAT IS ALREADY KNOWN ON THIS TOPIC

⇒ The primary concern for further clinical trials of bromodomain containing 4 (BRD4) inhibitors is the drug resistance. Also, limited responsive rate restricted the clinical application of immune checkpoint blockade (ICB) in cancers.

WHAT THIS STUDY ADDS

⇒ Our results raise an interesting possibility that transient therapy with BRD4 inhibitors (BRD4i) could induce a persistent mismatch repair deficiency phenotype with acquisition of a mutational profile that could sensitize patients to ICB.

HOW THIS STUDY MIGHT AFFECT RESEARCH, PRACTICE OR POLICY

⇒ These These results suggest potential routes forward that could combat the resistance to BRD4i by combining with ICB and allow fulfillment of the promise of BRD4i in clinical practice.

INTRODUCTION

The DNA mismatch repair (MMR) system maintains DNA replication fidelity and thus genetic integrity and stability. MMR

system consists of four core proteins: mutL homologue 1 (MLH1), PMS1 homolog 2 (PMS2), mutS homologue 2 (MSH2), and mutS homologue 6 (MSH6).[1] MMR deficiency (dMMR) occurs when MMR proteins are deficient or non-functional due to mutation. Tumors with dMMR typically have an increased tumor mutation burden (TMB), neoantigens, and immunogenicity that renders tumors sensitivity to immune checkpoint blockade (ICB) with anti-programmed death/ligand 1 (anti-PD-1/PD-L1) therapy in many tumor lineages, including melanoma, non-small cell lung cancer, and colorectal cancer.[2] Thus, dMMR is an established tumor lineage-independent biomarker for ICB with anti-PD-1/PD-L1.[3–7] However, less than 15% of patients across all tumor types are dMMR.[8] Therefore, several strategies, such as inactivating MLH1 through genome editing technology[9] or BRAF or EGFR inhibitors in BRAF-mutated colorectal cancer[10] can convert tumors from MMR-proficient (pMMR) to dMMR status with the hope of improving tumor response to ICB by inducing genetic instability and increasing mutability. However, translating genome editing technologies to the clinic faces major challenges, primarily in terms of the safety and efficacy of these treatments, and the effects of EGFR or BRAF inhibitors on MMR were restricted to BRAF-mutant cancers. Therefore, the development of another approach to induce dMMR status and render a broad population of patients responsive to anti-PD-1/PD-L1 is urgently needed.

Bromodomain containing 4 (BRD4), a member of the bromodomain and extraterminal domain protein family, translates signal-dependent chromatin alterations into gene expression readouts.[11] Preclinical studies have highlighted the impact of BRD4 inhibitors (BRD4i) as potent antitumor agents, which has led to the development of clinical trials involving BRD4i as single agents or in combination with existing treatment options in multiple human cancers (NCT01587703, NCT03059147, NCT02419417, NCT01949883, NCT03068351, and NCT02259114). The anticancer effects of BRD4i have been proposed to be due to downregulation of BRD4 target genes, and, in particular, *MYC*. However, downregulation of individual genes or gene signatures has proven insufficient to explain the magnitude of phenotypic effects conferred by BRD4i.[12 13] For example, ectopic overexpression of MYC only partially rescues BRD4i-mediated inhibition of prostate cancer cell growth.[12] Thus, the mechanisms underlying the effects of BRD4i on tumors remain largely unknown limiting the utility of BRD4i due to a lack of selection biomarkers and rational drug combinations.

Here, we found BRD4 inhibition transcriptionally inhibited MMR genes (MLH1, MSH2, MSH6, PMS2) expression, dampened MMR function, and increased dMMR mutation signatures both in vitro and in vivo. Furthermore, we demonstrated that BRD4i effectively induced dMMR in pMMR cells as well as in multiple BRD4i-resistant in vitro and in vivo tumor models. Importantly, the induced dMMR status rendered BRD4i sensitive and resistant parental pMMR tumors responsive to anti-PD-L1 monotherapy and combinational therapy. This is particularly important as patients who develop resistance to BRD4i could continue to benefit from immunotherapy.

RESULTS

BRD4 and MMR proteins expression are correlated across cancer lineages

BRD4 has been implicated in multiple DNA repair pathways including our transcriptional, proteomic, and functional analysis implicated BRD4 as a regulator of the homologous recombination repair pathway.[14] We thus explored whether BRD4 could contribute to other DNA damage repair pathways and demonstrated that BRD4 messenger RNA (mRNA) expression was positively correlated with the expression of MMR genes (MLH1, MSH2, MSH6, PMS2) in the majority of cancer types in The Cancer Genome Atlas (TCGA) (figure 1A). BRD4 and MSH6 and MSH2 protein, as assessed by reverse phase protein arrays (RPPA), were also correlated across cancer lineages with the exception of cholangiocarcinoma, kidney chromophobe and liver hepatocellular carcinoma (figure 1B). Similar correlations were observed in Clinical Proteomic Tumor Analysis Consortium (CPTAC) mass spectrometry data across assessed lineages except for colon adenocarcinoma (COAD) (figure 1C). BRD4 amplification happens most commonly in ovarian cancers (OVs). Thus, we further confirmed the correlations between BRD4 and MLH1, MSH2, MSH6, and PMS2 by immunohistochemistry (IHC) analysis of 70 high-grade serous OVs (figure 1D, p=0.0005).

BRD4 inhibition downregulated MMR proteins and impaired MMR function in vitro

Given that the mutSα protein complex (MSH2/MSH6) and mutLα complex (MLH1/PMS2) are both critical to MMR function,[15] reduction or malfunction of any of MLH1, MSH2, MSH6, and PMS2 is expected to lead to loss of MMR function.[16] To assess whether BRD4 inhibition could modulate the expression of genes involved in MMR, we exposed nine cell lines derived from diverse lineages (OV (A2780, SKOV3, and ID8); colorectal cancer (LoVo, CT26, and MC38); lung cancer (A549); cervical cancer (SiHa); melanoma (B16)) to AZD5153, a novel bivalent selective BRD4i,[17] and then examined the expression of MLH1, MSH2, MSH6 and PMS2 (figure 2A, online supplemental figure S1A). mRNA of these MMR-related genes was downregulated across the cell lines although the degree of decrease varied across cell lines (figure 2A, online supplemental figure S1A). In addition, analysis of public data sets confirmed that BRD4i (JQ1 and IBET-151) downregulated expression of MMR-related genes in MM1.S and SEM cells (GSE44929 and GSE139436, online supplemental figure S1B) that led to elevated dMMR scores[18] (online supplemental figure S1C).

Consistent with the mRNA results, AZD5153 also decreased levels of MLH1, MSH2, MSH6, and PMS2, once

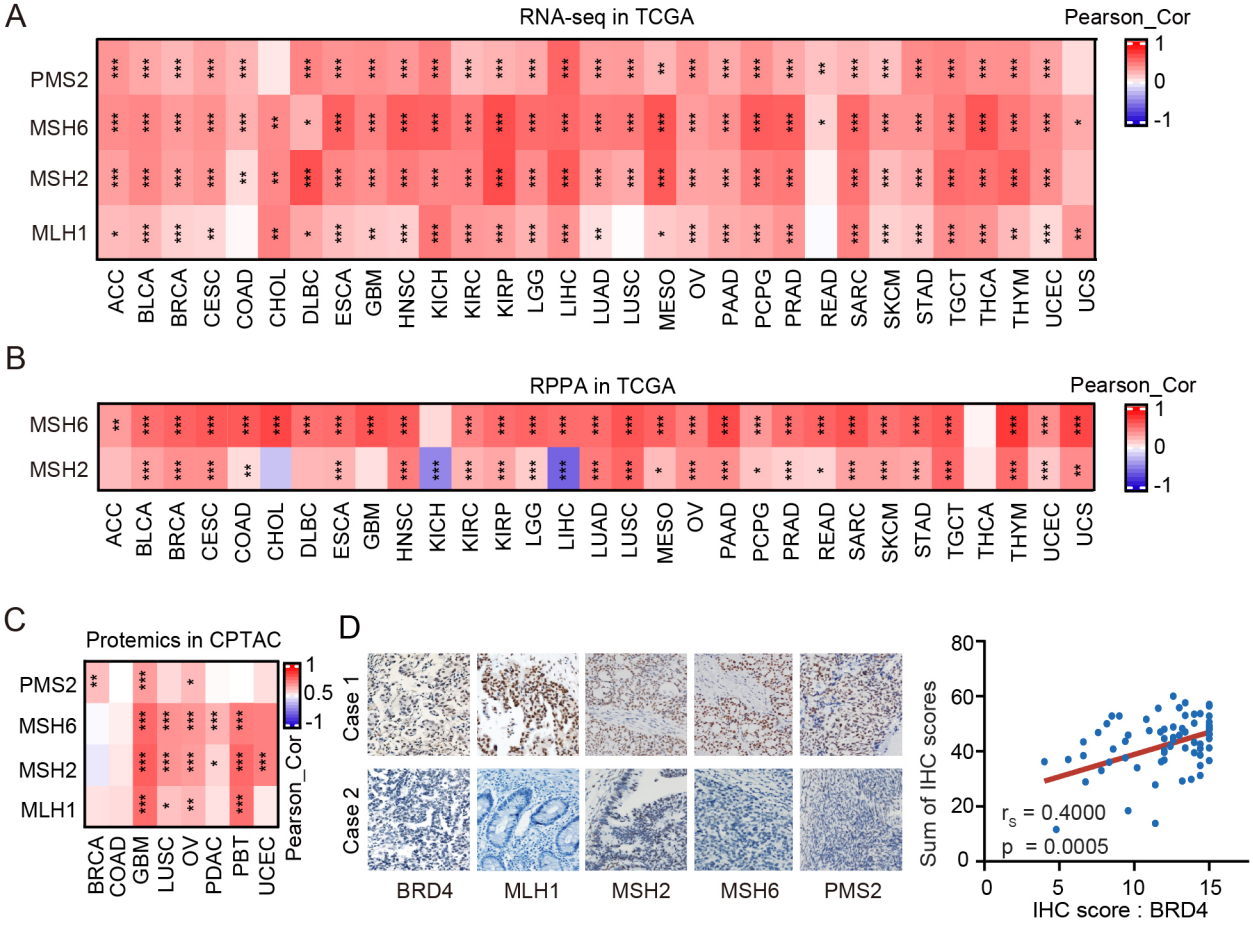

Figure 1 BRD4 and mismatch repair proteins expression are correlated across cancer lineages (A–B) mRNA expression (A) and protein levels (B) data in TCGA pan-cancer were obtained and the correlations of mRNA expression between BRD4 with MLH1, MSH2, MSH6, and PMS2 (A), and the correlations of protein levels of BRD4 with MSH2 and MSH6 were performed by Pearson's correlation analyses (B). Color indicates coefficients calculated by Pearson's correlation test (*, p<0.05; **, p<0.01; ***, p<0.001). (C) Proteomics data in CPTAC data was obtained and Pearson's correlation analyses of BRD4 with MLH1, MSH2, MSH6, and PMS2 was performed. Color indicates coefficients calculated by Pearson's correlation test (*, p<0.05; **, p<0.01; ***, p<0.001). (D) Representative IHC images (200×) of BRD4, MLH1, MSH2, MSH6, and PMS2 (left) and correlation between BRD4 IHC score and the sum of MLH1, MSH2, MSH6, and PMS2 IHC scores (right) in high-grade serous ovarian cancer tissues. ACC, adrenocortical carcinoma; BLCA, bladder urothelial carcinoma; BRCA, breast invasive carcinoma; BRD4, bromodomain containing 4; CESC, cervical squamous cell carcinoma and endocervical adenocarcinoma; CHOL, cholangiocarcinoma; COAD, colon adenocarcinoma; CPTAC, Clinical Proteomic Tumor Analysis Consortium; DLBC, lymphoid neoplasm diffuse large B-cell lymphoma; ESCA, esophageal carcinoma; GBM, glioblastoma multiforme; HNSC, head and neck squamous cell carcinoma; IHC, immunohistochemistry; KICH, kidney chromophobe; KIRC, kidney renal clear cell carcinoma; KIRP, kidney renal papillary cell carcinoma; LGG, brain lower grade glioma; LIHC, liver hepatocellular carcinoma; LUAD, lung adenocarcinoma; LUSC, lung squamous cell carcinoma; MESO, mesothelioma; MLH1, mutL homologue 1; mRNA, messenger RNA; MSH2, mutS homologue 2; MSH6, mutS homologue 6; OV, ovarian cancer; PAAD, pancreatic adenocarcinoma; PCPG, pheochromocytoma and paraganglioma; PMS2, PMS1 homolog 2, mismatch repair system component; PRAD, prostate adenocarcinoma; READ, rectum adenocarcinoma; RPPA, reverse phase protein arrays; SARC, sarcoma; SKCM, skin cutaneous melanoma; STAD, stomach adenocarcinoma; TCGA, The Cancer Genome Atlas; TGCT, testicular germ cell tumors; THCA, thyroid carcinoma; THYM, thymoma; UCEC, uterine corpus endometrial carcinoma; UCS, uterine carcinosarcoma.

again with variable levels of decrease across the cell lines assessed (figure 2B, online supplemental figure S1D). To exclude off-target effects of AZD5153, we applied CRISPR/Cas9 to knockout *Brd4* in ID8 cells and found reduced expression of MMR proteins, although with more modest effects than AZD5153 on MSH2 and MLH1 levels (figure 2C).

We subsequently directly assessed MMR function using a fluorescence-based multiplex host cell reactivation assay that measures the ability of human cells to repair G:G mismatch-containing plasmid reporters resulting in a gain in fluorescence[19] with decreases in G:G MMR being an indicator of dMMR.[20] HEK-293 cells treated with or without AZD5153 were transfected with G:G mismatch-containing plasmids. Following transfection of G:G mismatch-containing plasmids, AZD5153 markedly decreased fluorescence (figure 2D–E) indicative of AZD5253 inducing dMMR.

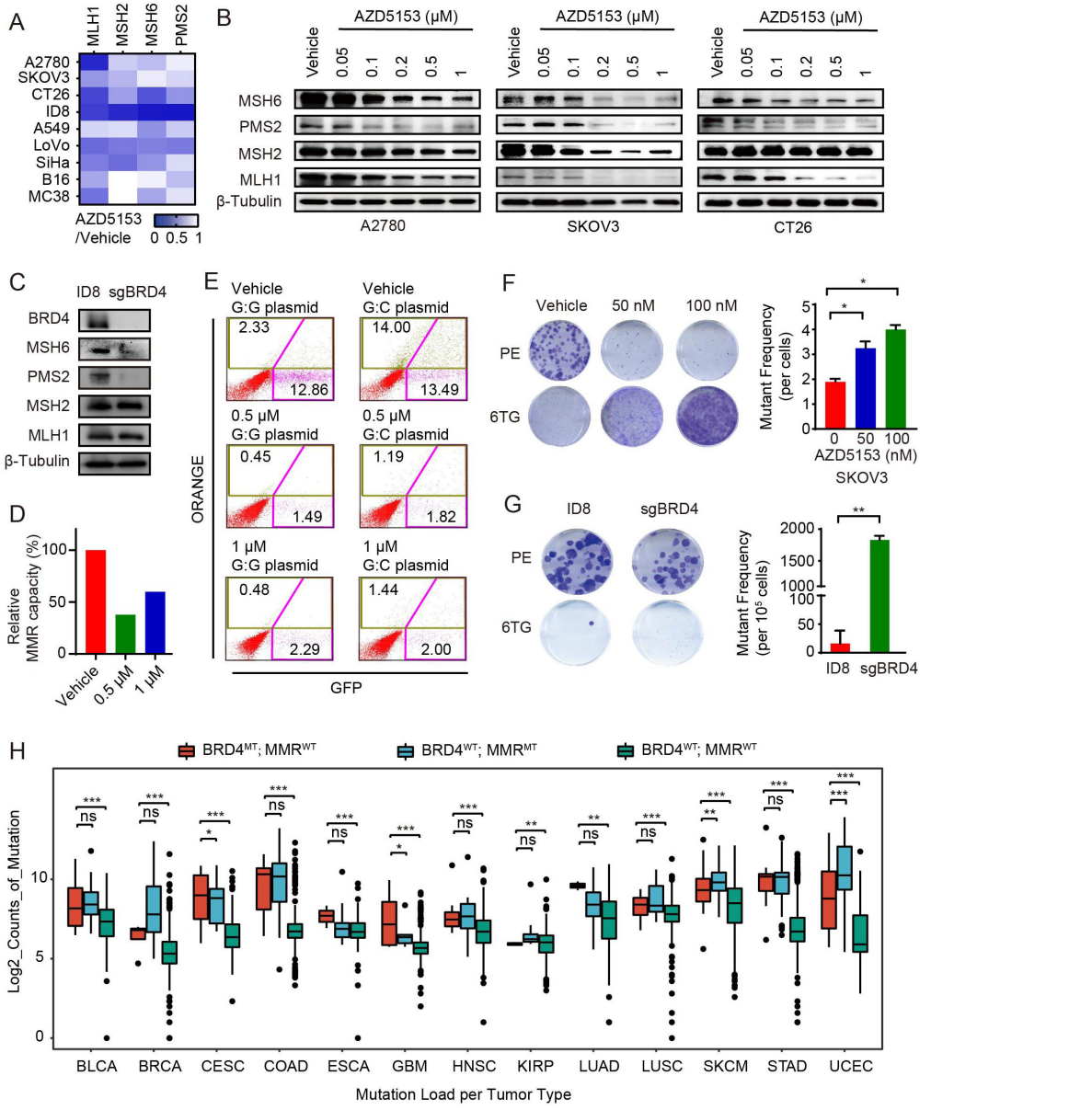

Figure 2 BRD4 inhibition downregulated MMR proteins and impaired MMR function in vitro (A) Heatmap showed relative expression changes of MLH1, MSH2, MSH6, and PMS2 by RT-qPCR in A2780, SKOV3, CT26, ID8, A549, LoVo, SiHa, B16, and MC38 cell lines treated with 1 μM AZD5153 for 48 hours. (B) Western blot of MLH1, MSH2, MSH6, and PMS2 proteins in A2780, SKOV3, and CT26 cell lines treated with the indicated doses of AZD5153 for 72 hours. (C) Western blot of BRD4 and MMR (MLH1, MSH2, MSH6, and PMS2) proteins in *Brd4* knockout ID8 cells and the parental ID8 cells. (D) Relative MMR capacities in HEK-293 cells treated with or without the indicated dose of AZD5153. (E) Representative pictures for MMR capacities in (D). (F) Representative pictures (left) and mutant frequency (right) of mutability assay in SKOV3 treated with vehicle or the indicated dose of AZD5153. The mutant frequencies were derived from hypoxanthine-guanine phosphoribosyl transferase gene mutation (6-TG sensitivity) assay. The mutant frequency refers to the numbers of mutated clones after normalized by PE. PE, plating efficiency; 6-TG, 6-thioguanine-treated samples. (G) Representative pictures (left) and mutant frequency (right) of mutability assay for *Brd4* knockout ID8 and the parental cells. (H) Mutation load (log2 mutation counts) in BRD4 mutant but MMR genes wild-type tumors ($BRD4^{MT}$; MMR^{WT}), BRD4 wild-type but MMR genes mutant tumors ($BRD4^{WT}$; MMR^{MT}), and BRD4 and MMR genes wild-type tumors ($BRD4^{WT}$; MMR^{WT}) from 15 cancer types based on The Cancer Genome Atlas data. MMR^{WT} indicates that at least one of four MMR genes (MLH1, MSH2, MSH6 and PMS2) is mutant. Data is shown as median and quartile, two-tailed t-tests (*, p<0.05; **, p<0.01; ***, p<0.001) Data is shown as mean±SEM, two-tailed t-tests (*, p<0.05; **, p<0.01; ***, p<0.001) in F–G. RT-qPCR, quantitative reverse transcription PCR**;** BLCA, bladder urothelial carcinoma; BRCA, breast invasive carcinoma; BRD4, bromodomain containing 4; CESC, cervical squamous cell carcinoma and endocervical adenocarcinoma; COAD, colon adenocarcinoma; ESCA, esophageal carcinoma; GBM, glioblastoma multiforme; HNSC, head and neck squamous cell carcinoma; KIRP, kidney renal papillary cell carcinoma; LUAD, lung adenocarcinoma; LUSC, lung squamous cell carcinoma; MLH1, mutL homologue 1; MMR, mismatch repair; MSH2, mutS homologue 2; MSH6, mutS homologue 6; PMS2, PMS1 homolog 2, mismatch repair system component; SKCM, skin cutaneous melanoma; STAD, stomach adenocarcinoma; UCEC, uterine corpus endometrial carcinoma.

MMR dysfunction results in a high mutation rate.[21] Cells that lose hypoxanthine-guanine phosphoribosyl transferase (HPRT) enzyme survive in the presence of 6-thioguanine (6-TG).[22] Importantly, AZD5153 rendered cells resistant to 6-TG in a concentration-dependent manner consistent with the induction of mutagenesis (figure 2F, online supplemental figure S1E). Furthermore, *Brd4* knockout in ID8 cells lead to a 10-fold increase in the number of cells that survived 6-TG compared with parental ID8 cells (figure 2G).

Decreased DNA damage repair in dMMR tumors leads to accumulation of DNA mutations.[3 5] Consistent with this concept, the numbers of mutation counts were significantly elevated in *BRD4* wild-type but MMR genes-mutated tumors compare to *BRD4* and MMR genes wild-type tumors across multiple tumor lineages (figure 2H). More interestingly, compared with *BRD4* and MMR genes-wild-type tumors, *BRD4*-mutanted but MMR genes-wild-type tumors exhibited a comparable increase in the number of mutation counts to *BRD4*-wild-type but *MMR* genes-mutated tumors (figure 2H).

Collectively, the data indicated that BRD4 inhibition, deletion, or mutation downregulates MMR proteins, resulting in dMMR and TMB elevation in multiple cancer types.

BRD4 transcriptionally regulates MMR genes

BRD4 regulates gene transcription by binding to acetylated histones and transcription factors.[23] Disruption of bromodomain-histone acetylation (H3K27 acetylation, etc) interactions by BRD4i results in decreased BRD4 binding to regulatory regions of target genes, reducing target genes expression.[24] To verify whether BRD4 directly regulates MMR genes transcription, we first identified BRD4-binding peaks at the promoter regions of *MLH1*, *MSH2*, *MSH6,* and *PMS2* genes in SUM159PT cells by analyzing published BRD4 chromatin immunoprecipitation-sequencing (ChIP-seq) data collected in the Cistrome Data Browser (figure 3A, online supplemental figure S2A).[25] Then we performed ChIP followed by quantitative PCR (qPCR) (ChIP-qPCR) in SKOV3 cells treated or untreated with AZD5153. A known BRD4 binding site in the promoter region of *c-Myc* was used as a positive control for the ChIP assays.[12] PCR-primers in non-enriched regions based on the above BRD4 ChIP-seq data served as a negative control (online supplemental figure S2B). ChIP-qPCR using a BRD4 antibody confirmed binding of BRD4 at the promoters of *MLH1*, *MSH2*, *MSH6,* and *PMS2* (figure 3B). Moreover, AZD5153 markedly decreased the binding (figure 3B). External ChIP-seq data sets confirmed the effects of JQ1 on binding of BRD4 at the promoters of MMR genes to be concentration-dependent in MM1.S (GSE44931,[26] figure 3C) and JQ1 also decreased the binding of BRD4 at the promoters of MMR in both parental and JQ1 resistant SUM149 or SUM159 cells (GSE131102,[27] figure 3D, online supplemental figure S2C). Taken together, these data suggested that BRD4 inhibition suppressed the transcription of MMR genes by blocking BRD4 protein binding to acetylated histones in regulatory regions of the MMR genes.

BRD4 inhibition decreases MMR proteins in multiple in vivo tumor models

To determine whether the cell-based findings can be exploited in tumor samples, we exploited our tumor biobank of patient-derived xenograft (PDX) models. The BRD4i JQ1 decreased tumor growth in a breast cancer PDX (figure 4A). We then assessed protein changes by RPPA analysis and found that MMR proteins, including MSH2, MSH6, and PMS2 were all markedly reduced in JQ1-treated tumors (figure 4B). IHC staining confirmed that JQ1 decreased PMS2, MSH2, and MSH6 (figure 4C). Consistent with the observation in breast cancer PDX, 15 days and 35 days treatment with AZD5153 decreased the growth of two high-grade serous OV PDX models (figure 4D–E). Again, AZD5153 decreased MMR proteins in the OV PDXs (MLH1, MSH2, MSH6, and PMS2 in PDX-OV-11; MLH1 and MSH2 in PDX-OV-9) (figure 4F–G). In the CT26 syngeneic mouse model, 15 days of treatment with AZD5153 decreased tumor growth although modestly compared with the PDX models (figure 4H). Once again protein levels of MSH2, MSH6, MLH1 (modestly), and PMS2 were diminished (figure 4I). Taken together, BRD4i suppressed the expression of MMR proteins in multiple in vivo tumor models.

Prolonged incubation with BRD4i in vitro results in acquisition of dMMR, a dMMR mutational signature that persists despite BRD4i resistance

The emergence of resistance remains a key challenge to cancer therapy. We therefore investigated whether the induced-dMMR status would be maintained in BRD4i resistant cells. SKOV3, A2780, CT26, and ID8 cells were challenged with increasing concentrations of AZD5153 for up to 4 months (figure 5A). The resultant AZD5153-resistant cell lines (SKOV3R, A2780R, CT26R, and ID8R) showed a 15–20-fold increase in half-maximal inhibitory concentration (IC50) (figure 5B). Despite the induction of resistance to the growth inhibitory effects of AZD5153, RNA sequencing (RNA-seq) analysis revealed a decrease in MMR genes in SKOV3R, A2780R, and ID8R cells after 2 months of drug exposure (figure 5C, online supplemental figure S3A). We next performed PreMSIm (predicting microsatellite instability (MSI) from mRNA) analysis[28] to infer the MSI status of AZD5153-treated cells. As expected, compared with parental cells, AZD5153-treated cells were defined as MSI-high at all treatment times (figure 5D, online supplemental figure S3B). The dMMR scores were upregulated at 24 hours and maintained for 4 months of BRD4i treatment despite the resistance of A2780R, SKOV3R, and ID8R to the growth inhibitory effects of BRD4i (figure 5E, online supplemental figure S3C). Moreover, at least one MMR protein was downregulated in AZD5153-resistant cells including

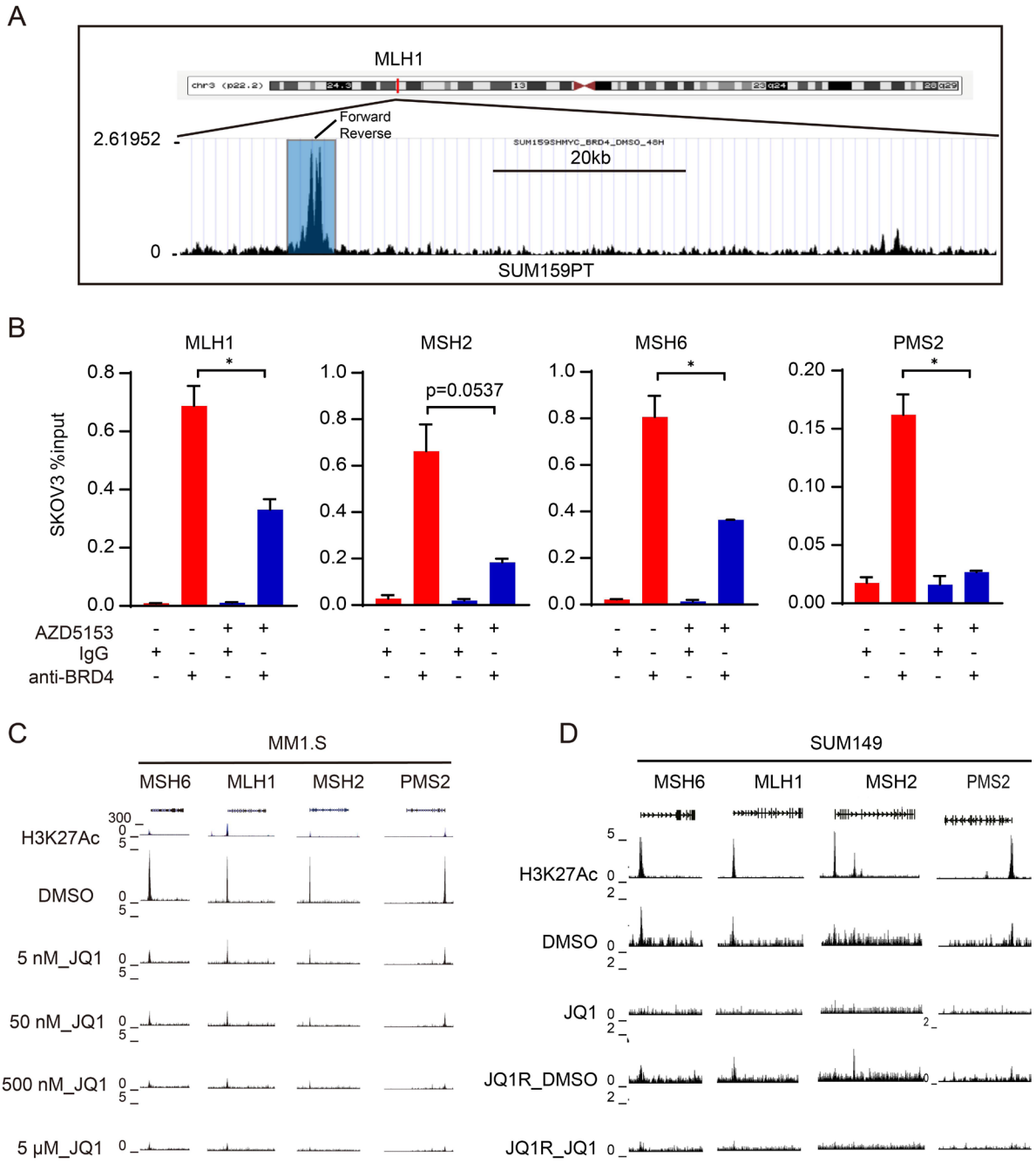

Figure 3 BRD4 transcriptionally regulates mismatch repair genes (A) UCSC Genome Browser was used to show BRD4 ChIP sequencing signal profiles in the MLH1 gene locus. Primers for ChIP-qPCR validation were indicated. (B) ChIP-qPCR of BRD4 in SKOV3 treated with vehicle or 1 µM AZD5135 for 48 hours. Data is shown as mean±SEM from each of three independent replicates. Two-tailed t-tests: *, p<0.05; **, p<0.01; ***, p<0.001. (C) ChIP sequencing showed BRD4 binding at the MLH1, MSH2, MSH6, and PMS2 loci in MM1.S cells treated with DMSO or the indicated dose of JQ1 in GSE44931 data set. (D) ChIP sequencing showed BRD4 binding at the MLH1, MSH2, MSH6, and PMS2 loci in SUM149 and JQ1-resistant (JQ1R) SUM149 cells treated with DMSO or 10 µM JQ1 in GSE131102 data set. BRD4, bromodomain containing 4; ChIP, chromatin immunoprecipitation; MLH1, mutL homologue 1; MSH2, mutS homologue 2; MSH6, mutS homologue 6; PMS2, PMS1 homolog 2, mismatch repair system component; qPCR, quantitative PCR; DMSO, Dimethyl sulfoxide.

PMS2 in A2780R and MSH6 in SKOV3R, CT26R, and ID8R (figure 5F).

Prolonged dMMR would be expected to result in the accumulation of mutations with a signature of dMMR. Indeed, AZD5153 increased the proportion of dMMR signatures compared with total mutation signatures in SKOV3R, A2780R, and ID8R cells with the increase being time dependent in SKOV3R (figure 5G) and induced to maximal levels at 1 month and retained over time in A2780R and ID8R cells (online supplemental figure S3D). The elevated dMMR mutational signatures were associated with HPRT mutation as demonstrated by resistance

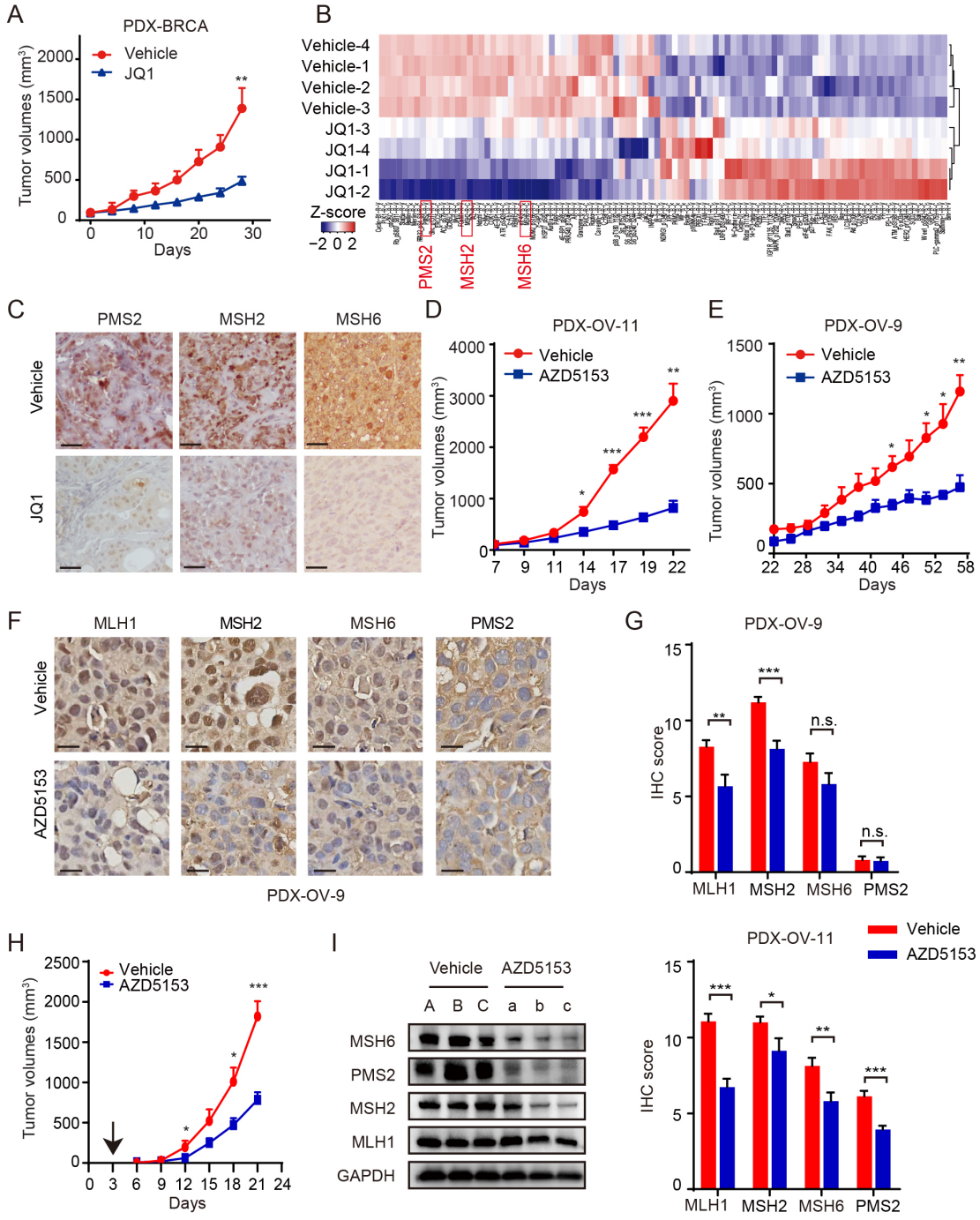

Figure 4 Bromodomain containing 4 inhibition decreases mismatch repair proteins in multiple in vivo tumor models (A) Tumor volume curves of breast cancer (BRCA) PDX mice treated with vehicle (n=4, 0.5% hydroxypropylmethylcellulose and 0.2% Tween 80) or JQ1 (n=4, 40 mg/kg per day, intraperitoneal) for 28 days. (B) Heatmap shows the z-score of reverse phase protein arrays data representing different levels of proteins in vehicle or JQ1 treatment samples from (A). (C) Tumor tissues from (A) were subjected to IHC analyses and probed with indicated antibodies. Representative images of IHC (200X) are shown with treatment indicated. (D and E) Tumor volume curves of OV-11 PDX (D) (n=4 mice) and OV-9 PDX (E) (n=3 mice) mice treated with vehicle (0.5% hydroxypropylmethylcellulose and 0.2% Tween 80) or AZD5153 (1.25 mg/kg per day, oral gavage). (F) OV-9 PDX mice treated with vehicle (0.5% hydroxypropylmethylcellulose and 0.2% Tween 80) or AZD5153 (1.25 mg/kg per day, oral gavage) and tumor tissues were collected and subjected to IHC analyses after treatment completed. Representative images of IHC of MLH1, MSH2, MSH6, and PMS2 proteins were shown. (Scale bar, 10 mm.) (G) Quantification of IHC scores (MLH1, MSH2, MSH6, and PMS2) in tumors with vehicle or AZD5153 treatment from OV-11 PDX (left) and OV-9 PDX right). (H) Tumor volume curves of CT26 xenografts mice treated with vehicle (n=5, 0.5% hydroxypropylmethylcellulose and 0.2% Tween 80) or AZD5153 (n=5, 1.25 mg/kg per day, oral gavage). (I) Western blots showing MLH1, MSH2, MSH6, and PMS2 proteins expression in tumor tissues from (H). Data represent mean±SD. Two-tailed t-tests: *, p<0.05; **, p<0.01; ***, p<0.001; n.s., not significant in A, D, E, G and H. IHC, immunohistochemistry; MLH1, mutL homologue 1; MSH2, mutS homologue 2; MSH6, mutS homologue 6; PDX, patient-derived xenograft; PMS2, PMS1 homolog 2, mismatch repair system component.

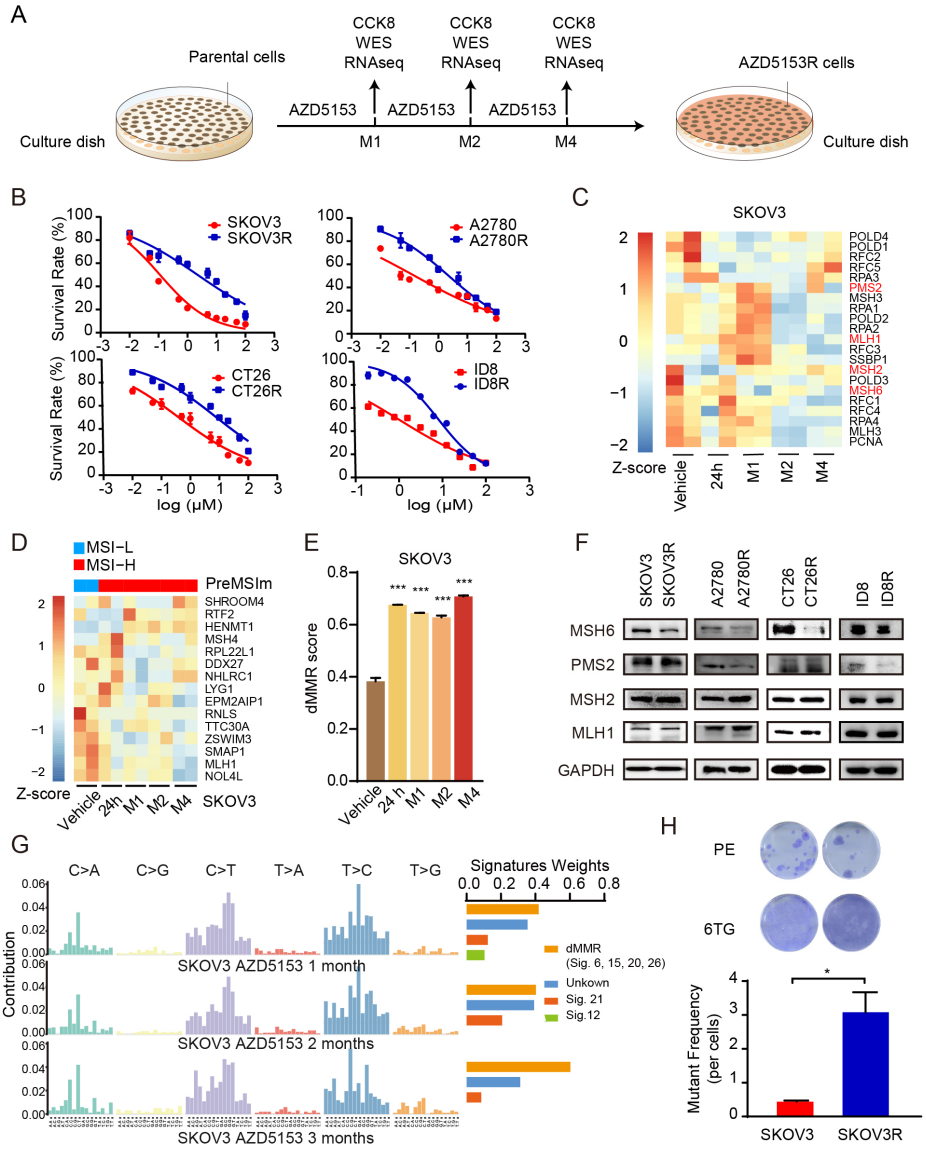

Figure 5 Prolonged incubation with BRD4i in vitro results in acquisition of dMMR, a dMMR mutational signature that persists despite BRD4i resistance (A) Schematic diagram of the establishment of AZD5153-resistant cell lines. Parental cells were subjected to gradual increases in AZD5153 concentrations until cells grew in the presence of 15–20-fold half-maximal inhibitory concentration (2–4 months from initial exposure). Samples were collected at 24 hours, 1 month, 2 month, and 4 month for RNA-seq and WES. AZD5153-induced cells with massive resistance after 2–4-month exposure were recognized as AZD5153R cell lines. (B) Cell viability curves of parental or AZD5153-resistant (A2780R (M2), SKOV3R (M4), CT26R (M4), and ID8R (M4)) cells treated with AZD5153 for 48 hours. Representative results are presented as means±SEM of three independent experiments. (C) RNA-seq data from SKOV3 cells treated with vehicle or AZD5153 (24 hours, 1 month, 2 months, and 4 months) were analyzed for the expression of 23 MMR-related genes. Heatmap shows z-score of relative expression of 23 MMR-related genes in indicated treatment. (D) RNA-seq data from SKOV3 cells treated with vehicle or AZD5153 (24 hours, 1 month, 2 months, and 4 months) were analyzed for PreMSIm signature to assess the MSI status. Heatmap shows z-score of relative expression of genes in indicated time point of AZD5153 treatment. The top bar indicates the MSI status defined by PreMSIm (blue indicates MSI-low (MSI-L), representing MMR-proficient; red indicates MSI-high (MSI-H), representing dMMR). (E) RNA-seq data from SKOV3 cells treated with vehicle or AZD5153 (24 hours, 1 month, 2 months, and 4 months) were analyzed for dMMR scores. Data represent mean±SD, two-tailed t-tests: *, p<0.05; **, p<0.01; ***, p<0.001. (F) Western blotting of MLH1, MSH2, MSH6, and PMS2 expression levels in A2780R (M2), SKOV3R (M4), and CT26R (M4) cells and their parental cells. (G) WES data from SKOV3 cells treated with vehicle or AZD5153 (1 month, 2 months, and 4 months) were analyzed for the mutational signature and the weights of known mutational processes in the COSMIC Signatures for each sample. The proportion of dMMR mutation signatures represented the sum of weights for dMMR-related COSMIC Signatures at each time point. (H) Representative pictures (upper) and mutant frequency (lower) of mutability assay in parental SKOV3 cells and SKOV3R (M4) cells. Data is shown as mean±SEM from each of three independent replicates, two-tailed t-tests: *, p<0.05; **, p<0.01; ***, p<0.001. BRD4i, bromodomain containing 4 inhibitors; dMMR, MMR deficiency; MLH1, mutL homologue 1; MMR, mismatch repair; MSH2, mutS homologue 2; MSH6, mutS homologue 6; MSI, microsatellite instability; PE, plating efficiency; PMS2, PMS1 homolog 2, mismatch repair system component; RNA-seq, RNA sequencing; WES, Whole Exome Sequencing; 6-TG, 6-thioguanine.

of SKOV3R and A2780R cells to 6-TG (figure 5H, online supplemental figure 1S3E).

Together, these results demonstrate that prolonged incubation with BRD4i results in persistent dMMR and acquisition of increased mutations. This suggested that prolonged treatment with BRD4i could result in sensitivity to ICB in syngeneic models.

AZD5153-resistant tumors acquire sensitivity to αPD-L1

We thus tested the contention that the dMMR status and accumulations of mutations that accompany prolonged incubation with AZD5153 would render BRD4-resistant CT26R cells sensitive to ICB (figure 6A). As previously reported,[29] parental CT26 cells are resistant to αPD-L1 monotherapy (figure 6B–C). Parental CT26 tumor growth was markedly decreased by AZD5153 alone or in combination with αPD-L1 (figure 6C). CT26R was modestly less sensitive to AZD5153 than parental CT26 (figure 6C), consistent with modest resistance in vitro (figure 5B). As expected, CT26R cells obtained accumulation of mutations taking the parental CT26 cell line as reference (online supplemental figure S4A), and CT26R-derived tumors were markedly sensitized to αPD-L1 (figure 6C). The combination of AZD5153 and αPD-L1 was more effective than monotherapy with either drug in CT26R perhaps due to the residual activity of AZD5153 in CT26R (figure 6C). No significant changes in body weight were observed, indicating the overall safety of the therapy (online supplemental figure S4B). As predicted by the persistent dMMR phenotype in the CT26R cells in vitro (figure 5D–F), the dMMR phenotype persisted in vivo in vehicle-treated cells with marked downregulation of MSH6 and PMS2 (figure 6D). Additionally, we found MMR proteins remained low in CT26R tumors, indicating that sensitivity to αPD-L1 may be related to reduced MMR proteins (figure 6D).

Multicolor flow cytometry (online supplemental figure S4C) demonstrated that αPD-L1 markedly increased the proportion of cytotoxic T cells ($CD8^+$ interferon (IFN)-γ^+) (figure 6E) and decreased the proportion of exhausted $CD8^+$ T ($TIM\text{-}3^+$ $PD\text{-}1^+$ $CD8^+$) cells (figure 6F) in CT26R compared with parental CT26 consistent with the effects on tumor growth. Thus, the increased sensitivity of CT26R to αPD-L1 may be due to the persistent dMMR and mutational status enhancing immunogenicity.

Prolonged exposure to BRD4i in vivo results in acquisition of dMMR, and BRD4i resistance and acquired sensitivity to αPD-L1 therapy

To construct a more clinically representative BRD4i-resistance model in vivo, we performed four rounds of CT26 tumor growth with or without AZD5153 treatment to create CT26I (vehicle-treated) and CT26RI (AZD5153-treated) (figure 7A). In contrast to the CT26R cells developed in vitro, the resultant CT26RI tumors were completely resistant to AZD5153 (online supplemental figure S5A). As with the CT26R model, the CT26RI cells exhibited persistent downregulation of MMR-related proteins with marked decreases in MSH6 and PMS2 despite resistance to the growth inhibitory effects of AZD5153 (online supplemental figure S5B). In a further transplant generation, CT26I (figure 7B,C, online supplemental figure 1S5C) demonstrated similar responses to mono and combination therapy with AZD5153 and αPD-L1 as parental CT26 (figure 6B,C). As predicted, CT26RI was completely resistant to AZD5153 (figure 7B,C). Strikingly, CT26RI was markedly sensitized to αPD-L1 that was augmented slightly, although not significantly, by AZD5153 (figure 7B,C, online supplemental figure S5C). No significant changes in body weight were observed, once again indicating the overall safety of the therapy (online supplemental figure S5D).

The dMMR phenotype persisted in CT26RI with marked downregulation of MSH6 and PMS2 (online supplemental figure S5E). Correspondingly, the tumor mutation counts were significantly elevated in CT26RI tumors (figure 7D). Flow cytometry (online supplemental figure S5F,G) did not demonstrate the increase in $PD\text{-}L1^+$ $CD45^-$ tumor cells in the CT26RI tumor cells that was observed in the CT26R model, however, AZD5153, αPD-L1, and the combination markedly downregulated $PD\text{-}L1^+$ tumor cells (figure 7E). As with CT26R, AZD5153, αPD-L1, and the combination markedly increased the proportion of cytotoxic T cells ($CD8^+$ IFN-γ^+) and decreased the proportion of exhausted $CD8^+$ T ($TIM\text{-}3^+$ $PD\text{-}1^+$ $CD8^+$) cells (figure 7F,G). This was further associated with a decrease in regulatory T cells in CT26RI on treatments (figure 7H).

The responses of CT26R and CT26RI are consistent with the contention that persistent dMMR and accumulation of mutations in chronically treated cells results in increased immunogenicity and sensitivity to αPD-L1 therapy.

DISCUSSION

dMMR predicts response of solid tumors to PD-1/PD-L1 blockade.[7] Although approximately 30% of endometrial cancers and 20% of the colon or gastric cancers are dMMR, in most other tumor types, less than 5% of tumors are dMMR.[30] Therefore, the development of strategies to induce dMMR and expand the utility of anti-PD-1/PD-L1 in pMMR tumors is urgently needed. In this study, we demonstrated that targeting BRD4 downregulated MMR genes expression and decreased MMR function resulting in accumulation of mutations and a dMMR signature through cellular, proteomic, and genomic assays, as well as in both in vitro and in vivo models. The ability of AZD5153 to reduce MMR expression appeared to be due to interruption of the effects of BRD4 on transcriptional regulation of MMR genes. BRD4i-resistant models generated in vitro and in vivo maintained a dMMR status despite resistance to growth inhibition by BRD4i. Strikingly, the persistent dMMR status and the accumulation of mutations led to the emergence of a therapeutic vulnerability to αPD-L1 therapy. Together the results indicate that combination therapy with BRD4i and ICB

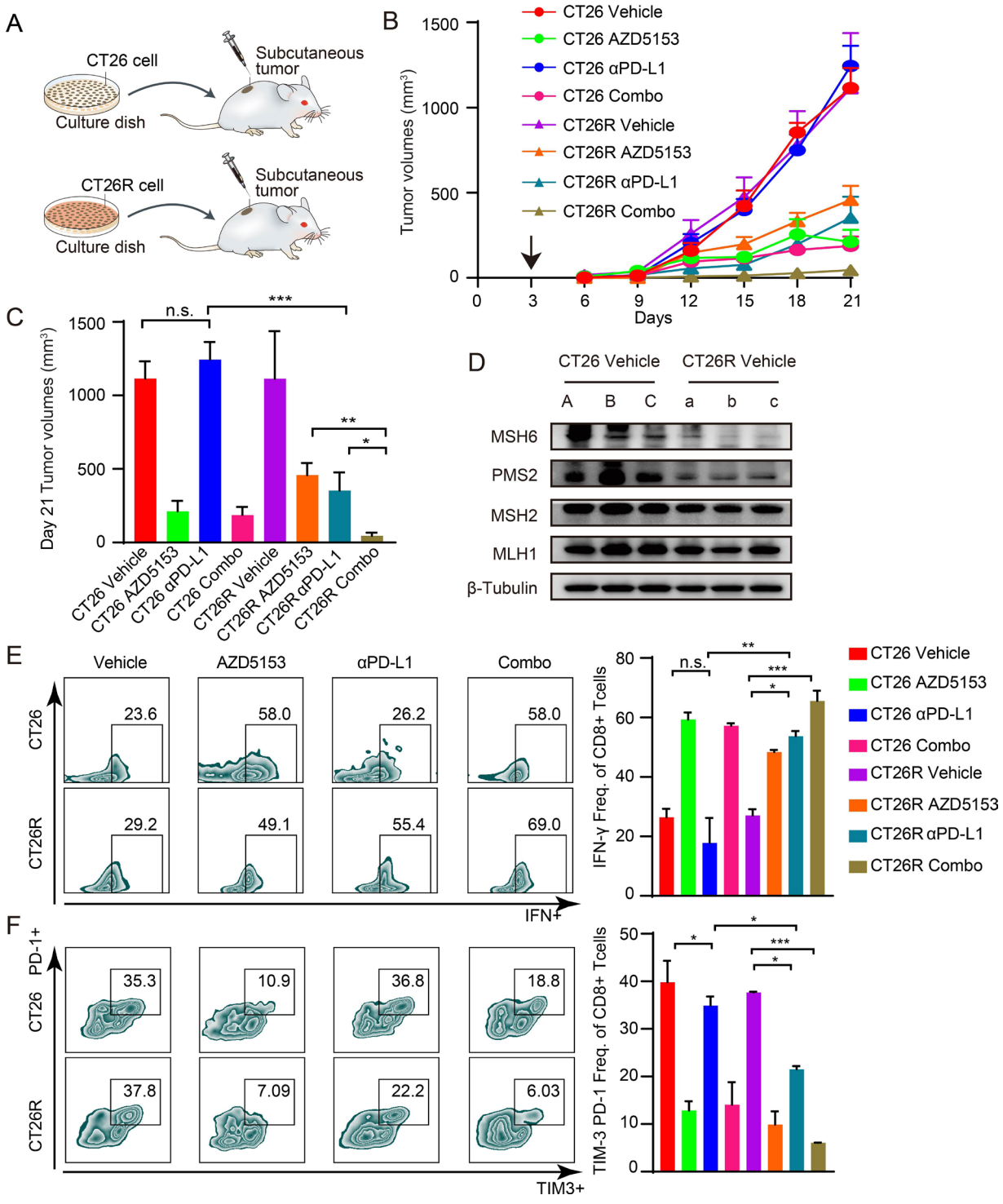

Figure 6 AZD5153-resistant tumors acquires sensitivity to αPD-L1 (A) Schematic diagram shows CT26 and CT26R cells were injected into BALB/c mice to establish the in vivo models. (B) CT26 and CT26R cells were injected into BALB/c mice. Three days later, mice were randomized into treatment cohorts: Vehicle (n=5, 0.5% hydroxypropylmethylcellulose and 0.2% Tween 80), AZD5153 (n=5, 1.25 mg/kg per day, oral gavage), αPD-L1 antibody (n=5, 200 µg/mouse every 3 days for six times), or a combination of AZD5153 and αPD-L1 antibody (n=5). Average tumor volumes±SEM for each cohort were displayed. (C) Tumor volumes on day 21 of (B). Data represent mean±SEM. Analysis of variance (ANOVA) was used to compare differences among multiple groups: *, p<0.05; **, p<0.01; ***, p<0.001; n.s., not significant. (D) Western blotting of MLH1, MSH2, MSH6, and PMS2 expression levels in CT26 and CT26R mice treated with vehicle. (E–F) Representative flow cytometry plots (left) and quantification of effector CD8 T cells ($CD8^+$ IFN-γ^+) (right) (E), exhausted CD8 T cells ($TIM3^+PD\text{-}1^+$) (F). T cells proportions of all $CD8^+$ T cells in tumors from each group, respectively (n=3). Data represent mean±SEM. P values were determined by ANOVA. *, p<0.05; **, p<0.01; ***, p<0.001. IFN, interferon; TIM-3, T cell immunoglobulin and mucin domain 3; MLH1, mutL homologue 1; MSH2, mutS homologue 2; MSH6, mutS homologue 6; n.s., not significant; PD-1, programmed death; PD-L1, programmed death ligand 1; PMS2, PMS1 homolog 2, mismatch repair system component.

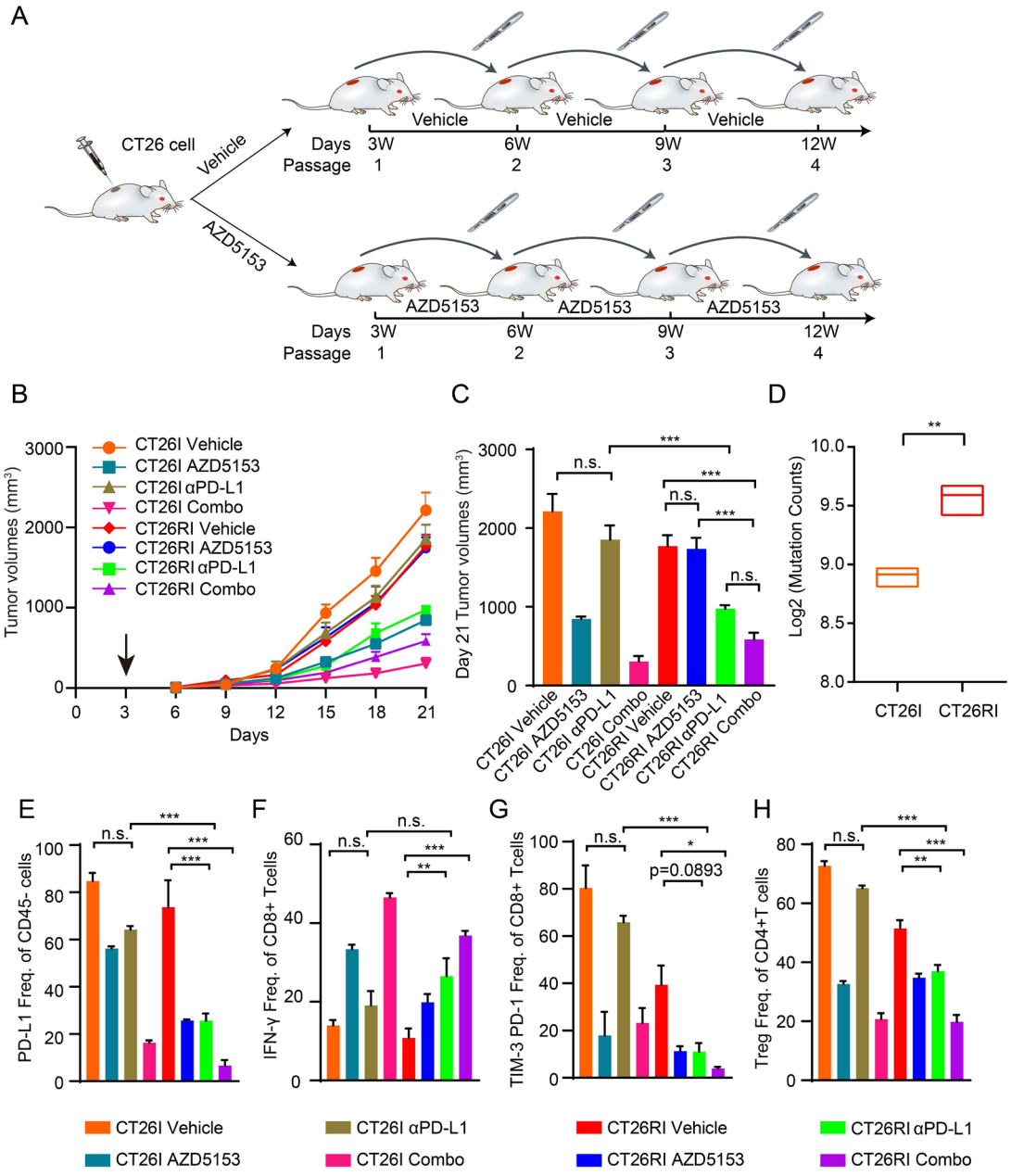

Figure 7 Prolonged exposure to BRD4i in vivo results in acquisition of dMMR, and BRD4i resistance and acquired sensitivity to αPD-L1 therapy (A) Scheme for the process of establishing of AZD515 resistant model in vivo (CT26RI) and the control model (CT26I). We first subcutaneously injected CT26 cells into BALB/c mice to establish the first-generation tumors. After 3 weeks of AZD5153 treatment, the remaining CT26 tumor tissues were transplanted into new BALB/c mice to construct the next generation tumors in vivo. Ultimately, a stable AZD5153-induced resistance in vivo model (CT26RI) and the control model (CT26I) were established after four rounds with or without continuous AZD5153 treatment until the growth of the CT26RI models was not suppressed by AZD5153 treatment. (B) We transplanted the tumor tissues with the same tumor sizes from the fourth generation of CT26I and CT26RI mice into 20 new BALB/c mice, respectively. Tumors of CT26I and CT26RI were further randomized into various treatment groups after implantation: Vehicle (n=5, 0.5% hydroxypropylmethylcellulose and 0.2% Tween 80), AZD5153 (n=5, 1.25 mg/kg per day, oral gavage), αPD-L1 antibody (n=5, 200 µg/mouse every 3 days for six times), or a combination of AZD5153 and αPD-L1 antibody (n=5). Average tumor volumes±SEM for each cohort is displayed. (C) Tumor volumes on day 21 of (B). Data represent mean±SEM. Analysis of variance (ANOVA) was used to compare differences among multiple groups: *, p<0.05; **, p<0.01; ***, p<0.001; n.s., not significant. (D) Tumor mutation counts derived from somatic variants by WES in CT26I and CT26RI tumors (n=3). (E–H) Quantification of PD-L1$^+$ tumor cells (gated on CD45$^-$ cells) (E), effector CD8 T cells (CD8$^+$ IFN-γ$^+$, gated on CD8$^+$ cells) (F), exhausted CD8 T cells (TIM-3$^+$ PD-1$^+$, gated on CD8$^+$ cells) (G), and Treg cells (FOXP3$^+$ CD25$^+$, gated on CD4$^+$ cells) (H) in CT26I and CT26RI tumors from each group, respectively (n=3) Data represent mean±SEM. P values were determined by ANOVA. *, p<0.05; **, p<0.01; ***, p<0.001. BRD4i, bromodomain containing 4 inhibitors; dMMR, deficiency mismatch repair; WES, Whole Exome Sequencing; IFN, interferon; TIM-3, T cell immunoglobulin and mucin domain 3; n.s., not significant; PD-1, programmed death; PD-L1, programmed death ligand 1; Treg, regulatory T cells.

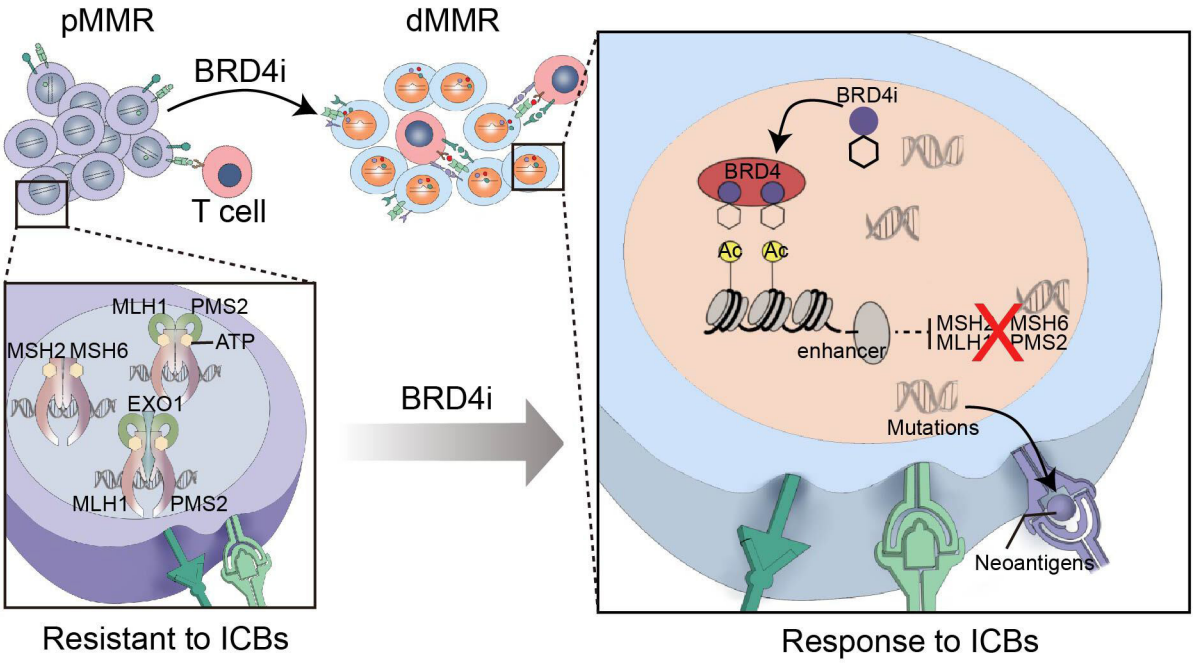

Figure 8 Graphical abstract. pMMR tumors with adequate mismatch repair proteins (MLH1, PMS2, MSH2, MSH6, etc.) are resistant to ICBs. BRD4 inhibition transcriptionally decreases the expression of MMR genes in cancer cells, thus promotes cancers acquiring a mutational profile that could sensitize patients to ICBs. MMR, mismatch repair; pMMR, proficient MMR; dMMR, deficient MMR; BRD4, bromodomain containing 4; ICB, immune checkpoint blockade.

with anti-PD-L1 capitalizes on an emergent therapeutic vulnerability that could increase antitumor activity and importantly prevent the emergence of BRD4i resistance or reverse it once it occurs.

EGFR/BRAF inhibition can induce DNA damage, trigger MSI, and lead to adaptive mutability in colorectal cancers that results in EGFR/BRAFi resistance.[10] However, it is not yet known whether dMMR status persists after acquisition of resistance and importantly whether this process leads to a new vulnerability to immunotherapy. The studies suggest that dMMR could contribute to BRD4i resistance. Importantly the sustained dMMR status even cells resistant to the growth inhibitory effects of BRD4i did lead to acquired vulnerability to immunotherapy.

Despite promising preclinical data toxicity of BRD4i has resulted in the termination of multiple BRD4i programs in industry,[31 32] our results raise an interesting possibility that transient therapy with BRD4i could induce a persistent dMMR phenotype with acquisition of a mutational profile that could sensitize patients to ICB (figure 8). Furthermore, our data indicates that continued therapy with BRD4i or combination therapy with BRD4i is not required for the increased responsiveness to ICB with anti-PD-L1. Together, these studies suggest potential routes forward that could ameliorate the toxicity of BRD4i and allow fulfillment of the promise of BRD4i in clinical practice.

Our study had some limitations. AZD5153-mediated reduction in MMR-related transcripts and proteins varied across the different cell lines. However, we are unable to determine the specificity and selectivity of BRD4 in regulating proteins within the MMR pathway. Moreover, the biomarkers for biologic effects by AZD5153, such as drug response or biomarkers for further response to immunotherapy needs further investigation. Further, we could not dissociate the acquisition of MMR mutational signatures from the effects of persistent dMMR on the activity of PD-L1 in the CT26R and CT26RI models. Further, we have not determined why the combination of AZD5153 and αPD-L1 is more effective than monotherapy in the resistant CT26 models although it is likely that this is due to residual effects of BRD4i even in models resistant to the growth effects of BRD4i. Despite these limitations, our studies warrant exploration of combination therapy with BRD4i and ICB in clinical trials.

MATERIALS AND METHODS

Cell lines and cell culture

HEK-293, A2780, MC38, A549, CT26, Hela, LoVo, SiHa, and SKOV3 were obtained from the American Type Culture Collection. B16 was obtained from the Kunming cell bank. The murine OV cell line ID8, which was derived from spontaneous malignant transformation of C57BL/6 mouse ovarian surface epithelium cells, was a gift from K Roby (University of Kansas, Lawrence, KS). HEK-293, A549, B16, CT26, ID8, MC38, Hela, LoVo, and SiHa were cultured with Dulbecco's modified Eagle's medium. SKOV3 was cultured with McCoy's 5a medium and A2780 was cultured with Roswell Park Memorial Institute 1640 medium. Cells were routinely supplemented with fetal bovine serum 10% and antibiotics (100 U/mL penicillin and 100 mg/mL streptomycin) and were incubated in a 37°C air incubator with 5% CO_2. All cell lines were authenticated through short tandem repeat profiling and

tested monthly for *Mycoplasma* by PCR. Cell lines were not passaged more than 30 times.

Generation of AZD5153-resistant cells

To generate AZD5153-resistant cells, A2780, SKOV3, ID8, and CT26 were subjected to gradual increases in AZD5153 concentrations until cells grew in the presence of 15-fold to 20-fold IC50 (2–4 months from initial exposure). AZD5153-induced cells with massive resistance after 2–4-month exposure were recognized as AZD5153R cell lines.

Antibodies and compounds

BRD4 (ab128874), MLH1 (ab92312), MSH2 (ab70270), and PMS2 (ab110638) antibodies were from Abcam. GAPDH (A19056), β-tubulin (A12289), and PMS2 (A19928) antibodies were from ABclonal. MSH6 (GTX11661) antibody was from GeneTex. BRD4 (83375) antibody was from Cell Signaling Technology.

AZD5153 (S8344) and JQ1 (S6993) were from Selleck. Compounds were dissolved in Dimethyl sulfoxide (DMSO) and stored as 10 mmol/L aliquots at instruction temperature. Anti-PD-L1 antibody (BE0101, clone B7-H1) and IgG isotype control (BE0090) were from Bio X Cell.

Fixable Viability Stain (BV510), CD45 (APC-Cy7 30-F11), CD3 (PE), CD4 (BV605 RM4–5), CD8a (FITC), CD25 (PE-Cy7 PC61), Foxp3 (Alexa Fluor 647), IFN-γ (PerCP-Cy5.5 XMG1.2), PD-1 (BV650 J43), PD-L1 (BV786), Transcription Factor Buffer Set and The Leukocyte Activation Cocktail (Leuko Act Cktl with GolgiPlug) were from BD Biosciences. Mouse CD16/32, and TIM-3 (BV421) were from BioLegend.

Clinical specimens

Seventy high serous OV samples from Tongji Hospital were collected immediately after surgical resection and further fixed in 10% formalin, dehydrated, incubated in xylene, and embedded in paraffin for IHC staining. Two fresh OV patient's tumor fragments from Tongji Hospital (PDX-OV-9 and PDX-OV-11) were implanted into female NOD/SCID mice for establishing PDXs.

Animal models

The PDX-breast carcinoma (BRCA) model was transplanted in MD Anderson Cancer Center and approved by the Institutional Animal Care and Use Committee of the MDACC. Other animal studies were conducted with permission from the Ethics Committee of Tongji Hospital, Tongji Medical College, Huazhong University of Science and Technology (TJH-201903003). Female, 8-week-old, NOD/SCID mice and BALB/c mice were purchased from Jiangsu Jicui Yaokang Biotechnology, and housed in laminar flow cabinets under specific pathogen-free conditions. Tumor size and mouse weight were monitored every 3 days. Tumor volumes were calculated using the formula: tumor volume=1/2 (length×width^2). All animal experiments with these models were conducted in compliance with the National Institute of Health guidelines for animal research.

CT26 subcutaneous model

CT26 tumor cells (2×10^5) in 100 µL of phosphate-buffered saline (PBS) were subcutaneously injected into the right flank of BALB/c mice. On the third day after injection, the mice were randomly assigned to treatment cohorts as follows: vehicle, AZD5153 (1.25 mg/kg per day), αPD-L1 (200 µg/mouse every 3 days for six times), and the combination of AZD5153 and αPD-L1 (same doses as above). Mice weight and tumor volumes were examined every 3 days. The treatment was terminated on day 18 or the tumor diameter reached the maximum limit of 2 cm.

Generation of BRD4i-resistant models in vivo

To obtain a tumor in vivo model resistant to AZD5153, 2×10^5 CT26 cells were subcutaneously injected into 8-week-old female BALB/c mice (passage 0, P0). Mice were orally treated with vehicle or AZD5153 (1.25 mg/kg per day) starting on the third day of injection. Mice were examined every 3 days for their weight and tumor burden. Mice were sacrificed for tissue harvest when the maximum tumor burden reached 2000 mm^3. The tumor tissues were isolated into 1 mm^2 fragments and then transplanted into the new BALB/c mice, called passage 1 (P1). Then, the above steps were repeated four times. We transplanted the 1 mm^3 fragments of tumor tissues from the fourth generation of CT26I and CT26RI mice into 20 8-week-old female BALB/c mice, respectively. Both CT26I and CT26RI were randomized into four cohorts as follows: Vehicle, AZD5153, αPD-L1, and AZD5153/αPD-L1 combination (same doses as above).

PDXs models

Fresh human high serous OV tumor tissues were isolated into 5×5×5 mm^3 and subcutaneously implanted into 8-week-old female NOD/SCID mice. When tumors reached 1×1×1 cm^3, they were aseptically harvested and passed to the next generation.[33] The PDX models for drug screening were commonly the third passages, because the tumor take rate became approximately 100% through mouse-to-mouse passages in the third passages.

RPPA

Protein lysates were analyzed by RPPA supported by MDACC CCSG (Cancer Center Support Grant) as previously described.[34] Antibodies and approaches are referred to the RPPA website (https://www.mdanderson.org/research/research-resources/core-facilities/functional-proteomics-rppa-core.html).

IHC staining

Briefly, formalin-fixed paraffin-embedded tissue was subsequently sectioned at 4 µm and mounted on coated glass slides. Tissues were deparaffinized and antigen retrieved before antibody staining. Then stain with primary antibody overnight at 4°C. Primary antibodies included BRD4 (ab128874, working dilution 1:500), MLH1 (ab92312,

working dilution 1:200), MSH2 (ab70270, working dilution 1:500), MSH6 (GTX111661, working dilution 1:200), PMS2 (ab19928, working dilution 1:200). Normal serum was used as a negative control. Then, slides were observed under a microscope and pictures were taken in five areas (200×). Staining was semi quantitatively scored for intensity (0, no staining; 1, weak staining; 2, moderate staining; and 3, strong staining) and extent (0, no staining; 1, 1–25% staining; 2, 26–50% staining; 3, 51–75% staining; 4, 76–100% staining). Intensity and extent were multiplied to yield a score. Every score is evaluated individually and the mean of five readings was calculated for every slide. Staining score was determined separately by two experts under the same conditions. In rare cases, discordant scores were re-evaluated and scored by another expert.

Western blot analysis

Cells were lysed at 4°C for 30 min with RIPA buffer (Servicebio, G2002-100) supplemented with Protease Inhibitor Cocktail (Servicebio, G2006) and Phosphatase Inhibitor (Servicebio, G2007). Lysates were sonicated on ice and then centrifuged at 4°C for 30 min at 12,000 g. Supernatant has been collected and the protein concentration was measured by Coomassie (Beyotime, ST1119). Proteins were separated by 10% SDS-PAGE gels (BioSci, 8012011), and then electro-transferred onto 0.45 µm polyvinylidene difluoride membranes (Cytiva Life Sciences, 10600023). After blocking with 5% bovine serum albumin at room temperature for 1 hour, membranes were incubated with primary antibodies at 4°C overnight, followed by 1:5000 horseradish peroxidase conjugated secondary antibody (Antgene, ANT020) for 1 hour at room temperature. Bands were visualized using WesternBright ECL kit (Advansta, 190,113–13).

Quantitative reverse transcription PCR (RT-qPCR) assays

Total RNA (2 µg) was isolated using FastPure Cell/Tissue Total RNA Isolation Kit (Vazyme Biotech) and then reversely transcribed into complementary DNA with the HiScript Q-RT SuperMix for qPCR (Vazyme Biotech) according to the manufacture instructions. The SYBR Green Real-Time PCR Master Mixes kit was used for the thermocycling reaction in a Bio-Rad CFX96 Real-Time system. The mRNA levels analysis was carried out in triplicate and normalized by actin. Primers sequences are listed in online supplemental table S1.

MMR assay

The MMR assay was performed and referred to Nagel's study.[19] Briefly, 2.5×10^5 cells incubated in 6-well plastic culture plates were transfected with a mixture containing 700 ng of pmax-vector, 150 ng of pmax-BFP, and 150 ng pmax-mOrange (G:C undamaged control) or with pmax-G:G-mismatch containing-mOrange (damaged MMR) using Lipofectamine 3000 (Thermo Fisher Scientific, L3000015). After transfection, cells were treated with DMSO and AZD5153 (0.5 µM and 1 µM) for 6 hours and then analyzed by flow cytometry. The relative MMR capacity was calculated by dividing the percentage of mOrange positive cells in damaged MMR by the percentage of mOrange positive cells in undamaged control.

HPRT gene mutation (6-TG sensitivity) assay

$1\times10^4/1\times10^2$ cells were plated onto 6-well plates. After 24 hours, the high-density cells were cultured with medium containing 5 µg/L hypoxanthine. 1×10^2 cells were seeded in medium without hypoxanthine to obtain a plating efficiency (PE) at the time of selection. The cells were incubated for 14 days and stained with 0.5% crystal violet to observe the colony formation. The mutant frequency[22] was calculated according to the formula: $MF=a/(10^4\times(b/2\times10^2))$, where a=total number of 6-TG^r colonies and b=total number of colonies on 2 PE plates. MF assays were constructed in triplicate for statistical analysis.

ChIP-qPCR

Cells were cross-linked with 1% formaldehyde for 10 min at room temperature. The cross-linking reaction was stopped by adding glycine to a final concentration of 125 mM for 5 min. Cells were then lysed with a lysis buffer (50 mM Tris.HCl, 10 mM EDTA, 1% SDS, protease inhibitor cocktail, and 20 mM sodium butyrate). Chromatin was sheared to DNA fragments of 200–1000 bp by micrococcidase, and the lysate was sonicated and pelleted by centrifugation at 12,000× g, 4°C for 20 min. For immunoprecipitation, 1.5 µg BRD4 antibody (83375) or rabbit IgG control was incubated with sheared DNA overnight. The next day, samples were incubated with Protein A/G beads for 2 hours. DNA was then eluted, de-cross-linked, and purified. Each binding was assessed by ChIP-qPCR enrichment of loci. Data were normalized and calculated using per cent input: Adjusted Input=CtInput-log2 (Vchromatin/VInput), V means volume. % Input=100×2 (Adjusted Input – Ct Chromatin). Each group has three independent replicates. ChIP-qPCR primer sequences are listed in online supplemental table S2.

Chip-seq data analysis

ChIP-seq data for MM1.S, SUM149, and SUM159 cells were derived from GSE44931[26] and GSE131102[27] via the Cistrome Data Browser. Peak visualization and cross comparison were performed in the UCSC Genome Brower. Specifically, ChIP-seq for these cells treated with JQ1 and DMSO were compared with input.

Cytotoxicity measurement

Briefly, cells were seeded overnight in 96-well plates at a density of 3×10^3 cells / well. AZD5153 was diluted in DMSO and added to cells at concentrations of 0.01, 0.05, 0.1, 0.5, 1, 5, 10, 50 and 100 µM (200 µL/well, three replicates) for 48 hours. After that, each well was refilled with 100 µL fresh media supplemented with 10% Cell Counting Kit-8 analysis (Dojindo Laboratories, CK04) and incubated for 2 hours in the dark. Fresh media were used as a control.

The absorbance at 450 nm was measured with a microplate reader (Thermo Fisher Science, New York City, USA). The analysis was performed by GraphPad Prism V.8.3.0.

RNA-seq strategy

Cell lines treated with AZD5153 (1 µM) at several time points (24 hours, 1 month, 2 months, and 4 months) and vehicles were collected for RNA isolation, with two biological replicates. Library construction was performed using 1 µg RNA per sample using VAHTS mRNA sequencing V.2 Library Prep Kit for Illumina following manufacturer's recommendations. The libraries were sequenced on an Illumina NovaSeq platform to generate 150 bp paired-end reads, according to the manufacturer's instructions. The clean reads were mapped to the reference genome using HISAT2 (V.2.0.4). Bowtie2 (V.2.2.5) was applied to align the clean reads to the reference coding gene set then the expression level of the gene was calculated by RSEM (V.1.2.12).

dMMR score, and predicting MSI from mRNA analysis (PreMSIm)

The heatmap for MMR-related gene lists[35] was displayed by the pheatmap package from the R platform (V.4.2.0). dMMR scores were calculated by multiplying the z-normalized gene expression and corresponding coefficients and then dividing by the sum of the absolute values of all the gene coefficients. The predicting methods and the dMMR gene lists were provided in McGrail's study.[18] Additionally, we predicted the MMR status by the PreMSIm packages from the R platform (V.4.2.0).[28]

Whole exome sequencing (WES) and mutational signature analysis

All the AZD5153-induced cells and parental cells as above were collected, extracted, and quantified to 1 µg DNA for further library preparation and sequencing. Library construction was performed using Agilent SureSelect Human All Exon V.6 kit (Agilent Technologies, California, USA) following the manufacturer's recommendations. After cluster generation, the DNA libraries were sequenced on Illumina NovaSeq platform and 150 bp paired-end reads were generated. Clean data was aligned to the reference genome using Burrows-Wheeler Aligner (V.0.7.17). Picard (V.2.0.1) was used to remove duplicated sequence reads. Realignment was performed with the Genome Analysis Toolkit GATK (V.4.2.6.0). For BRD4i-resistant cell lines and mouse model, paired parental cell lines were used for calling variants in order to figure out drug-determined mutations. Somatic variants were called by MuTect (V.2)[36] on human cell lines, and Strelka V.2[37] on mouse cell lines and mouse tumor models. The weights of COSMIC Mutational Signatures (https://cancer.sanger.ac.uk/signatures/) contributing to each sample were concluded by the deconstructSigs package of the R platform (V.4.2.0). The proportion of dMMR mutation signatures was calculated by the sum of weights for dMMR-related COSMIC Signatures. Tumor mutation counts were calculated by the maftools package from the R platform (V.4.2.0).

Flow cytometry and intercellular cytokine staining

Tumor tissue was washed with PBS, cut into small pieces, and further incubated in dissociation tissue (Tumor Dissociation Kit, mouse, Miltenyi Biotec) at 37°C and 120 rpm for 40 min. The isolated cells were passed through a 40 µm filter to obtain a single-cell suspension, then red blood cells were lysed, and tumor tissue-associated lymphocytes were isolated by density centrifugation. After the cell count, the cells were placed in the incubator and pre-stimulated with stimulation blocker for 8 hours. The following monoclonal antibodies were used for flow cytometry: Fixable viability stain 700, anti-CD45, anti-CD3, anti-CD8a, anti-CD4, anti-CD274, anti-CD279, anti-CD25, and anti-TIM-3. The single cell suspension was stained in 100 µL PBS at 4°C for 15 min, and 1 µg/sample was stained with fluorescently labeled antibody. Intracellular cytokines, including anti-Foxp3 and anti-IFN-γ were fixed, permeabilized, and stained with a fixation/permeabilization kit. The single cell suspension after staining of tumor tissue was analyzed by flow cytometry with CytoFlex. Data were statistically analyzed using FlowJo V.10 software.

TCGA data analysis

TCGA pan-cancer gene expression data were downloaded from UCSC Xena (http://xena.ucsc.edu/). The cBioPortal for Cancer Genomics (http://cbioportal.org) was used to access the CPTAC data set, which includes studies of invasive BRCA, COAD, glioblastoma, lung squamous cell carcinoma, OV, pancreatic ductal adenocarcinoma, pediatric brain cancer and uterine corpus endometrial carcinoma. Pearson's correlations between MMR and BRD4 in the levels of both transcriptional profiles and RPPA data were calculated in each cancer species. The pan-cancer whole genome sequencing data were downloaded from UCSC Xena. BRD4 mutations were derived from Mutation Annotation Format files and tumor mutation counts were summarized by the maftools package of the R platform (V.4.2.0).

Statistical analysis

Two-sided student's t-test was used to compare differences between two groups of cells in vitro and in vivo. If the multiple groups data followed a normal distribution, we used analysis of variance test for multiple comparisons. Non-parametric pairwise comparisons (Mann-Whitney) were conducted where tumor size did not follow a Gaussian distribution in vivo. Data is presented as means±SEM and $p<0.05$ was considered significant. Statistical analyses were performed using the statistical package for the social sciences (SPSS) V.22.0 software and GraphPad Prism (V.8.0). Statistical parameters, including sample size and statistical significance, are reported in the figures and corresponding figure legends.

Author affiliations
[1]Department of Gynecological Oncology, Tongji Hospital of Tongji Medical College of Huazhong University of Science and Technology, Wuhan, Hubei, People's Republic of China
[2]National Clinical Research Center for Gynecology and Obstetrics, Tongji Hospital of Tongji Medical College of Huazhong University of Science and Technology, Wuhan, Hubei, People's Republic of China
[3]Department of Obstetrics and Gynecology, Zhongnan Hospital of Wuhan University, Wuhan, Hubei, People's Republic of China
[4]Department of Obstetrics and Gynecology, The First Affiliated Hospital of Shihezi University, Shihezi, Xinjiang, People's Republic of China
[5]Department of Stomatology, Tongji Hospital of Tongji Medical College of Huazhong University of Science and Technology, Wuhan, Hubei, People's Republic of China
[6]Department of Cell, Development and Cancer Biology, Oregon Health & Science University Knight Cancer Institute, Portland, Oregon, USA

Contributors CS is responsible for the overall content as the guarantor. YF, BY and YC contributed equally to this work. YF, BY and YC designed, performed, and analyzed experiments. XH, XL, FL, TQ, LZ, RX, WL, DH and JL verified and interpretated the results. ZH, JF, and WP assisted for sequencing and database analysis. YF, BY and YC finished drafting. EG, XQ, BW and GBM contributed to revising the manuscript. GC and CS contributed to the conception or design of the work and reviewed the draft critically for important intellectual content. All authors read and approved the manuscript.

Funding This study was supported by National Key R&D Program of China (2022YFC2704200, 2022YFC2704202), the Natural and Science Foundation of China (Nos. 81974408 (CS), 82073259 (GC), 82002762 (EG)), the Key Research and Development Program of Hubei Province (No.2020BCA067 (GC)).

Competing interests GBM is one of the SAB (Scientific Advisory Board) members or consults with AstraZeneca, Chrysallis Biotechnology, GSK, ImmunoMET, Ionis, Lilly, PDX Pharmaceuticals, Signalchem Lifesciences, Symphogen, Tarveda, Turbine, Zentalis Pharmaceuticals. GBM has stock options with Catena Pharmaceuticals, ImmunoMet, SignalChem, Tarveda.

Patient consent for publication Not applicable.

Ethics approval The usage of patient tumors in this study was approved by the Ethics or Institutional Review Board of Tongji Hospital (ethic ID: S1141), Tongji Medical College, Huazhong University of Science and Technology, China, in accordance with the Declaration of Helsinki. Participants gave informed consent to participate in the study before taking part.

Provenance and peer review Not commissioned; externally peer reviewed.

Data availability statement Data are available upon reasonable request.

ORCID iDs
Zhe Hu http://orcid.org/0000-0002-2724-6778
Chaoyang Sun http://orcid.org/0000-0003-2469-1638

REFERENCES

1 Gupta D, Heinen CD. The mismatch repair-dependent DNA damage response: mechanisms and implications. *DNA Repair (Amst)* 2019;78:60–9.
2 Yi M, Jiao D, Xu H, *et al*. Biomarkers for predicting efficacy of PD-1/PD-L1 inhibitors. *Mol Cancer* 2018;17:129.
3 Le DT, Uram JN, Wang H, *et al*. Pd-1 blockade in tumors with mismatch-repair deficiency. *N Engl J Med* 2015;372:2509–20.
4 Lin AY, Lin E. Programmed death 1 blockade, an achilles heel for MMR-deficient tumors? *J Hematol Oncol* 2015;8:124.
5 Dudley JC, Lin M-T, Le DT, *et al*. Microsatellite instability as a biomarker for PD-1 blockade. *Clin Cancer Res* 2016;22:813–20.
6 Graham LS, Montgomery B, Cheng HH, *et al*. Mismatch repair deficiency in metastatic prostate cancer: response to PD-1 blockade and standard therapies. *PLoS One* 2020;15:e0233260.
7 Le DT, Durham JN, Smith KN, *et al*. Mismatch repair deficiency predicts response of solid tumors to PD-1 blockade. *Science* 2017;357:409–13.
8 Lorenzi M, Amonkar M, Zhang J, *et al*. Epidemiology of microsatellite instability high (MSI-H) and deficient mismatch repair (dmmr) in solid tumors: a structured literature review. *Journal of Oncology* 2020;2020:1–17.
9 Germano G, Lamba S, Rospo G, *et al*. Inactivation of DNA repair triggers neoantigen generation and impairs tumour growth. *Nature* 2017;552:116–20.
10 Russo M, Crisafulli G, Sogari A, *et al*. Adaptive mutability of colorectal cancers in response to targeted therapies. *Science* 2019;366:1473–80.
11 Wu S-Y, Chiang C-M. The double bromodomain-containing chromatin adaptor Brd4 and transcriptional regulation. *J Biol Chem* 2007;282:13141–5.
12 Asangani IA, Dommeti VL, Wang X, *et al*. Therapeutic targeting of BET bromodomain proteins in castration-resistant prostate cancer. *Nature* 2014;510:278–82.
13 Wyce A, Degenhardt Y, Bai Y, *et al*. Inhibition of BET bromodomain proteins as a therapeutic approach in prostate cancer. *Oncotarget* 2013;4:2419–29.
14 Sun C, Yin J, Fang Y, *et al*. BRD4 inhibition is synthetic lethal with PARP inhibitors through the induction of homologous recombination deficiency. *Cancer Cell* 2018;33:401–16.
15 Jun SH, Kim TG, Ban C. Dna mismatch repair system. classical and fresh roles. *FEBS J* 2006;273:1609–19.
16 Sekine S, Mori T, Ogawa R, *et al*. Mismatch repair deficiency commonly precedes adenoma formation in Lynch syndrome-associated colorectal tumorigenesis. *Mod Pathol* 2017;30:1144–51.
17 Rhyasen GW, Hattersley MM, Yao Y, *et al*. AZD5153: a novel bivalent BET bromodomain inhibitor highly active against hematologic malignancies. *Mol Cancer Ther* 2016;15:2563–74.
18 McGrail DJ, Garnett J, Yin J, *et al*. Proteome instability is a therapeutic vulnerability in mismatch repair-deficient cancer. *Cancer Cell* 2020;37:371–86.
19 Nagel ZD, Margulies CM, Chaim IA, *et al*. Multiplexed DNA repair assays for multiple lesions and multiple doses via transcription inhibition and transcriptional mutagenesis. *Proc Natl Acad Sci U S A* 2014;111:E1823–32.
20 Parsons R, Li GM, Longley MJ, *et al*. Hypermutability and mismatch repair deficiency in RER+ tumor cells. *Cell* 1993;75:1227–36.
21 Zhao P, Li L, Jiang X, *et al*. Mismatch repair deficiency/microsatellite instability-high as a predictor for anti-PD-1/PD-L1 immunotherapy efficacy. *J Hematol Oncol* 2019;12:54.
22 Glaab WE, Tindall KR. Mutation rate at the HPRT locus in human cancer cell lines with specific mismatch repair-gene defects. *Carcinogenesis* 1997;18:1–8.
23 Donati B, Lorenzini E, Ciarrocchi A. Brd4 and cancer: going beyond transcriptional regulation. *Mol Cancer* 2018;17:164.
24 Zhang W, Prakash C, Sum C, *et al*. Bromodomain-Containing protein 4 (BRD4) regulates RNA polymerase II serine 2 phosphorylation in human CD4+ T cells. *J Biol Chem* 2012;287:43137–55.
25 Mei S, Qin Q, Wu Q, *et al*. Cistrome data browser: a data portal for ChIP-Seq and chromatin accessibility data in human and mouse. *Nucleic Acids Res* 2017;45:D658–62.
26 Lovén J, Hoke HA, Lin CY, *et al*. Selective inhibition of tumor oncogenes by disruption of super-enhancers. *Cell* 2013;153:320–34.
27 Shu S, Wu H-J, Ge JY, *et al*. Synthetic lethal and resistance interactions with BET bromodomain inhibitors in triple-negative breast cancer. *Mol Cell* 2020;78:1096–113.
28 Li L, Feng Q, Wang X. PreMSIm: an R package for predicting microsatellite instability from the expression profiling of a gene panel in cancer. *Comput Struct Biotechnol J* 2020;18:668–75.
29 Ho WW, Gomes-Santos IL, Aoki S, *et al*. Dendritic cell paucity in mismatch repair-proficient colorectal cancer liver metastases limits immune checkpoint blockade efficacy. *Proc Natl Acad Sci U S A* 2021;118:e2105323118.
30 Marcus L, Lemery SJ, Keegan P, *et al*. Fda approval summary: pembrolizumab for the treatment of microsatellite instability-high solid tumors. *Clin Cancer Res* 2019;25:3753–8.

31 Liang D, Yu Y, Ma Z. Novel strategies targeting bromodomain-containing protein 4 (BRD4) for cancer drug discovery. *Eur J Med Chem* 2020;200:112426.
32 Spriano F, Stathis A, Bertoni F. Targeting BET bromodomain proteins in cancer: the example of lymphomas. *Pharmacol Ther* 2020;215:107631.
33 Hidalgo M, Amant F, Biankin AV, *et al*. Patient-Derived xenograft models: an emerging platform for translational cancer research. *Cancer Discov* 2014;4:998–1013.
34 Paweletz CP, Charboneau L, Bichsel VE, *et al*. Reverse phase protein microarrays which capture disease progression show activation of pro-survival pathways at the cancer invasion front. *Oncogene* 2001;20:1981–9.
35 Seo I, Lee HW, Byun SJ, *et al*. Neoadjuvant chemoradiation alters biomarkers of anticancer immunotherapy responses in locally advanced rectal cancer. *J Immunother Cancer* 2021;9:e001610.
36 Cibulskis K, Lawrence MS, Carter SL, *et al*. Sensitive detection of somatic point mutations in impure and heterogeneous cancer samples. *Nat Biotechnol* 2013;31:213–9.
37 Saunders CT, Wong WSW, Swamy S, *et al*. Strelka: accurate somatic small-variant calling from sequenced tumor-normal sample pairs. *Bioinformatics* 2012;28:1811–7.